Laser Chem. 1988, Vol. 9, pp. 289–315

The State-selected Predissociation Dynamics of $CClF_2NO$ $\tilde{A}(n, \pi^*)$

MARTIN R. S. McCOUSTRA,† JULIE A. DYET‡ and JOSEF PFAB

Department of Chemistry, Heriot-Watt University, Riccarton, Edinburgh EH14 4AS

(Received 20 May, 1988)

The photodissociation of gaseous $CClF_2NO$ at 300 K and <20 K in a supersonic jet has been studied in the wavelength range 568 to 705 nm of the $S_1(n,\pi^*) \leftarrow S_0$ electronic transition. Energy disposal into, rates of formation and product-state distributions of the nascent $NO(X^2\Pi_i)$ photofragment have been measured in detail, and have been compared with statistical (Prior) calculations. The rotational population distributions of the NO fragment are statistical up to the highest excess energies investigated, while the spin-orbit branching ratios are very non-statistical and non-thermal, favouring the lower component. The lack of evidence for state-specific effects in the energy disposal and appearance times of the NO indicate that excess energy randomises prior to dissociation. Intersystem crossing to T_1 dominates the predissociation of all but the lowest S_1 levels. Levels close to the O,O origin predissociate either by internal conversion to the ground state or by vibrational predissociation on an S_1 potential energy surface that is weakly bound in the dissociation coordinate. A bond dissociation energy of 13 700 ± 350 cm^{-1} (164 kJ mol^{-1}) has been evaluated for the C—N bond.

KEY WORDS: Laser photochemistry, photofragmentation, jet spectroscopy, C-nitroso compounds.

INTRODUCTION

The last ten years have seen a dramatic revival of interest in the study of photofragmentation processes, that continues to be fuelled by rapid

† School of Chemical Sciences, University of East Anglia, Norwich NR4 7TJ.
‡ Proctor and Gamble (NTC), Whitley Road, Longbenton, Newcastle NE12 9TS.

experimental advances and accompanying progress in theoretical analysis.[1,2] This revival was initiated by the now classic work of Busch and Wilson on molecular beam laser photofragment spectroscopy[3] and later by the emergence of pulsed laser dissociation-probe techniques particularly the powerful laser-induced fluorescence (LIF) method.[1,4,5] The marriage of molecular beam and laser dissociation-probe techniques now offers an elegant and extremely informative experimental approach to studying photodissociation processes in microscopic detail, provided one of the fragments is amenable to probing by LIF or resonantly enhanced multiphoton ionisation (REMPI).

Among a wide variety of polyatomic species suitable for photodissociation-LIF probe studies, molecules producing the NO ground-state fragment are particularly promising candidates. The spectroscopy of the $A \leftarrow X$ Rydberg transition of NO is known in considerable detail, and both single- and two-photon LIF excitation spectra on this transition, commonly denoted the γ-band system of NO are well characterised.[5–7] The ground state of NO ($X^2\Pi_i$) is split by spin-orbit interaction giving rise to two rotational manifolds separated by roughly 120 cm^{-1}. Orbital-rotation interaction causes further fine-structure splitting of each rotational level into Λ-doublets that can be discriminated readily by means of the optical selection rules. Thus, LIF or (1 + 1) resonantly enhanced two-photon ionisation techniques permit detailed evaluation of electronic branching ratios, rotational, vibrational and fine-structure populations. In addition Doppler-profile studies can reveal energy and momentum disposal into translation.

In consequence considerable attention has focused recently on photodissociation studies of various nitroso-compounds.[8] Both predissociation following excitation via structured electronic absorption bands and fast, direct dissociation from repulsive upper electronic states have been studied using LIF of nascent NO.[9–14] The photodissociation of C-nitroso compounds in the visible in particular appears to provide textbook examples of slow predissociation processes. Such studies permit one to test theories of radiationless decay and of the unimolecular decomposition of long-lived complexes.[8–15]

The penetrating studies of Dixon and collaborators of the LIF excitation spectra and photophysics of HNO in the visible region have recently provided a detailed model for the spectroscopy and radi-

ationless decay of C-nitroso compounds excited on the $\tilde{A}\,^1A'' \leftarrow \tilde{X}^1A'$ (n,π^*) transition in the 500–720 nm region of the visible spectrum.[16,17] Near the dissociation threshold Renner–Teller coupling between the $\tilde{A}^1A''$ and $\tilde{X}^1A'$ states of HNO leads to rotationally assisted internal conversion (IC) to degenerate ground-state levels prior to dissociation. At higher energies, as the density of states in the intermediate $\tilde{a}^3A''$ state (T_1) becomes larger, dissociation from the triplet surface following spin-orbit induced intersystem crossing (ISC) becomes important.[17]

In seminal work on the photodissociation of CF_3NO Bower *et al.* demonstrated the power of supersonic jet-cooling in combination with pulsed dissociation-delayed LIF to achieve vibrational state-selection and to obtain detailed product-state distributions of the nascent NO $(X^2\Pi_i)$ fragment.[18] By varying the delay between dissociation and probe pulses they were able to show that the rates of appearance of NO equal the fluorescence lifetimes of $CF_3NO(\tilde{A}^1A'')$, and that they decrease monotonically with increasing excitation energy above the O_0^0 origin of the n,π^* absorption bands. They concluded that both the dissociation and fluorescence decay rates reflect the rates of internal conversion (IC) from S_1 levels to highly vibrationally excited levels of S_0, which then dissociate in a nearly statistical fashion on the S_0 surface.

In a more recent re-investigation of the spectroscopy, photophysics and photodissociation dynamics of CF_3NO we have demonstrated the influence of S_1–T_1 coupling of all but the lowest lying levels of the $\tilde{A}^1A''$ state. Our work has shown that the absence of significant deviations from statistical (Prior) product-state distributions cannot be taken as evidence for well-behaved, adiabatic unimolecular decay on the ground-state surface.[19] A clear example of the influence of ISC on the predissociation dynamics of C-nitroso compounds has been unravelled with jet-cooled $(CH_3)_3CNO$ by Noble *et al.*[20] Here excitation of parent features below a 650 cm^{-1} barrier above the dissociation threshold leads to slow unimolecular dissociation on the ground-state surface and statistical $NO(X^2\Pi_i)$ product-state distributions. Above this 650 cm^{-1} barrier prompt dissociation of $(CH_3)_3CNO$ produces non-statistical product-state distributions and is proposed to occur from the $\tilde{a}^3A''$ surface. This predissociation therefore proceeds in close analogy to the mechanism suggested by Dixon *et al.* for HNO and DNO,[16,17] but could be demonstrated beautifully with product-state distributions

and bi-exponential appearance rates of the nascent NO($X^2\Pi_i$) photofragment.[20]

As part of a systematic investigation of the spectroscopy, photophysics and predissociation dynamics of the $\tilde{A}^1A''$ states of C-nitroso compounds we present here studies of the dissociation dynamics of chlorodifluoronitroso-methane ($CClF_2NO$). Despite the lower symmetry, this molecule closely resembles CF_3NO revealing a very similar vibrationally structured $\tilde{A} \leftarrow \tilde{X}$ n,π^* electronic transition in the 500–700 nm wavelength region with similar oscillator strength. It predissociates like CF_3NO and $(CH_3)_3CNO$ as summarised in Eq. (1).

$$CClF_2NO\ (\tilde{X}) \xrightarrow{650nm} CClF_2NO\ (\tilde{A}\ n,\pi^*) \longrightarrow CClF_2 + NO(X^2\Pi_i) \quad (1)$$

EXPERIMENTAL

Synthesis of $CClF_2NO$

$CClF_2NO$ was prepared in a three-step synthesis starting with the vacuum pyrolysis of PTFE powder to produce tetra-fluoroethene. Addition of NO_2 to the olefin in the gas phase and subsequent hydrolysis of the addition products provides difluoronitroacetic acid. The decarboxylation of this acid with hot hydrochloric acid generates crude gaseous $CClF_2NO$. Various modifications of this synthesis and the purification of $CClF_2NO$ have been described in detail elsewhere.[21–24] The compound was stored at −20°C in the absence of light and air and repurified prior to use by several trap-to-trap distillations *in vacuo*. Infrared and visible absorption spectra of the blue gas were used to monitor its purity.

Room temperature photodissociation experiments

$CClF_2NO$ vapour at a pressure <150 mTorr was pumped slowly from a sample container kept near −100°C by means of a slush bath, through a small room temperature LIF flow cell. This cell was equipped with baffle arms, Suprasil I windows (Heraeus) for admission of the laser beams and for observing at right angle the UV-fluorescence of NO($A^2\Sigma^+$) excited by the probe laser. A Nd–YAG pumped dye laser (JK 2000) loaned from the laser support facility of the SERC provided the red dissociation beam with fixed wavelengths of 568 nm (Rhoda-

mine 6G in methanol) and 645 nm (DCM in methanol) at pulse energies of <25 mJ and <10 mJ, respectively. A planoconvex lens of 500 mm focal length focused the dissociation beam into the centre of the cell to a spot size of ca. 1.5 mm as judged from burn patterns. The probe laser, a Lambda-Physik EMG 50 excimer pumped dye laser (FL 2002) delivered between 0.5 to 1 mJ pulse energy for interrogation of nascent NO on the $A^2\Sigma^+ \leftarrow X^2\Pi_i$ transition using the dyes coumarin 47 and 107 in methanol. A Photon Control model 25 power meter and a Molectron pyroelectric detector (J3–05) continuously monitored the average pulse energies of dissociation and probe beams. A temporal delay of 100 ns between the dissociation and probe pulses was used unless specified otherwise resulting in a combined jitter of ± 20 ns. The pulse durations were 15 ns for the dissociation and 5 ns for the probe laser system. An in-house constructed multiple delay generator controlled the synchronisation of the lasers as described in the following section.

Photodissociation of jet-cooled $CClF_2NO$

The experimental set-up is shown in Figure 1. The expansion chamber consists of a small in-house constructed and anodised aluminium cube of 145 mm edge equipped with five 'O' ring sealed vacuum flanges and is mounted via a cylindrical Al pipe on a 100 mm liquid nitrogen trapped oil diffusion pump (Edwards EO4K and NTC 4). A quarter swing valve (Edwards QSB 100) between the top of the trap and the neck of the chamber allows the apparatus to be isolated from the diffusion and the mechanical rotary backing pump (Edwards E2M18). The chamber and its jet-cooling performance have been described in detail elsewhere.[25] Briefly, two identical light-collection telescopes are mounted by flanges on opposite faces of the cube. Suprasil I windows (Heraeus) transmit the fluorescence light collected by condensor lenses, that are positioned inside the chamber. One telescope images fluorescence in the visible and near-IR collected by an f/0.8 BK7 crown glass aspheric condensor lens (Spindler and Hoyer, Göttingen) onto the photocathode of a GaAs photomultiplier tube (RCA 4832). This serves to detect laser-excited fluorescence in the visible, while fluorescence from laser-excited $NO(A^2\Sigma)$ is collected by Suprasil–I optics (Heraeus) consisting of a doublet of planoconvex spherical lenses and a field lens, and is viewed through the opposite telescope by a solar

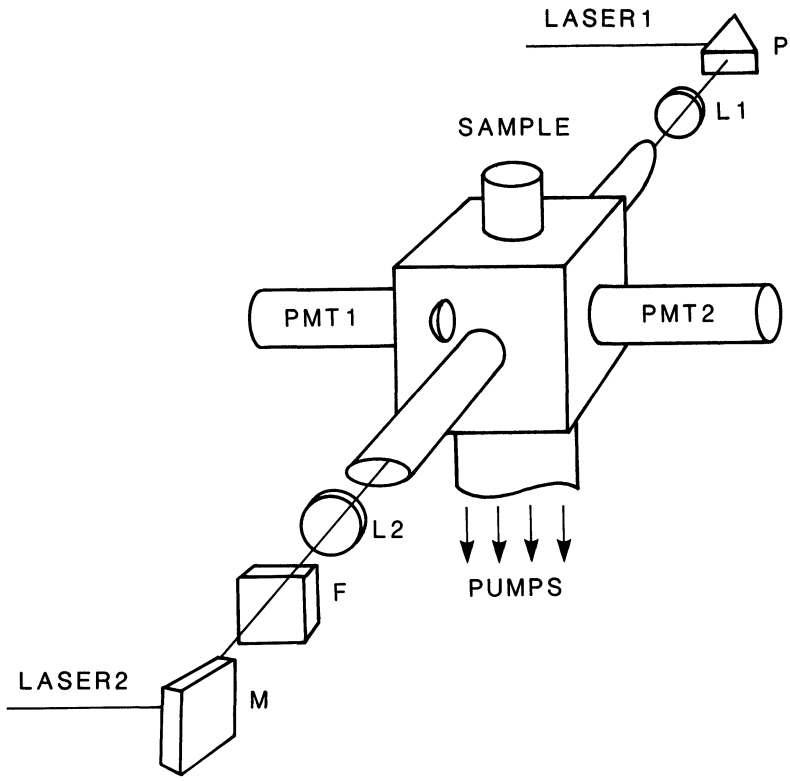

Figure 1 Artist's view of experimental set-up for dissociation-probe experiments of jet-cooled $CClF_2NO$, laser 1: dye laser beam for pulsed dissociation, laser 2: dye laser beam for pulsed delayed probing of NO by two-photon LIF on the γ-bands, P: prism, M: mirror, L_1 and L_2: lenses, F: glass blocking filter, PMT: photomultiplier tubes.

blind photomultiplier (Hamamatsu R166 UH). Filters (Schott RG 715 and UVR-250) are mounted in the telescopes, and baffles equipped with a series of conically shaped irises as well as Brewster-angled quartz windows serve to reduce scattered laser light.

A pulsed solenoid valve (NRC model BV-100) mounted in the centre of the top flange delivers gas pulses of 150 μs duration. During routine operation of the valve at 10 Hz pulse repetition rate and at 500 Torr stagnation pressure the chamber vacuum remains near 2×10^{-4} Torr. Under the same expansion conditions NO or NO_2 in mixtures of less than 1% by volume in Ar are cooled to a rotational temperature of less than 10 K.

The dissociation laser system (laser 1 in Figure 1) consisted of the same JK 2000 Nd–YAG pumped dye laser used for the room-temperature experiments and provided pulse energies <8 mJ in the 670–720 nm region with pyridine 1 in methanol or <12 mJ in the 600–680 nm region with DCM in methanol. The Lambda Physik EMG50/FL2002 coumarin dye laser (laser 2 in Figure 1) provided ca. 1 mJ for probing nascent NO on the two-photon γ-bands. The colinearly aligned and counter-propagating beams were focused by the lenses L1 (f = 500 mm) and L2 (f = 200 mm) such that their foci overlapped in the centre of the chamber and observation region ca 5 mm below the nozzle orifice. Suitable glass blocking filters prevent the dissociation beam from entering the probe dye laser. Mixtures of $CClF_2NO$ (5–10% by volume) with Ar were prepared on a glass vacuum line equipped with greaseless Teflon taps and an MKS baratron capacitance gauge. The mixtures were stored at 296 K in 5 dm^3 blackened glass bulks connected to the pulsed valve.

Signal acquisition and synchronisation of lasers

Our signal processing system consists of a 100 MHz 8 bit digital transient recorder (Transiac TR 2001) and crate controller housed in and powered by a Grenson CAMAC crate. Stray 308 nm light in the probe dye laser triggers signal acquisition under the control of an IBM–PC microcomputer using CAMAC commands to simulate gated detection and boxcar integration of transient fluorescence signals. A mains phase-locked and crystal-controlled oscillator built in-house acts as the master clock and provides TTL level pulses for the opening of the molecular beam valve, the firing of the Nd–YAG flash lamps, the triggering of the Q-switch and the firing of the excimer laser *via* an in-house constructed analogue multiple delay generator. The pulse repetition rate used was 10 Hz. Scanning of the dye laser grating may be controlled externally by computer or internally via a home-built stepper motor controller. Spectra can be corrected for variation of the dye laser output during extensive scans over a wide wavelength interval by the microcomputer. Such wide spectral scans are recorded using a gated integrator and boxcar averager (Stanford Research Systems) rather than the transient recorder. An A to D converter and the microcomputer in conjunction with a Hewlett–Packard digital plotter (HP7470) are employed for displaying spectra.

Electronic absorption spectra of $CClF_2NO$

The visible absorption spectrum of gaseous $CClF_2NO$ was recorded at a resolution of 2 Å with a dual-beam microprocessor controlled spectrophotometer (Shimadzu UV-240) using a 10 cm fused silica cylindrical cell. Molar extinction co-efficients were calculated using pressure readings from an MKS baratron gauge.

RESULTS AND ANALYSES

Spectroscopy of $CClF_2NO$

The electronic absorption spectrum of 9.95 Torr of $CClF_2NO$ vapour at 295 K is shown in Figure 2. We calculate a maximum molar decadic absorption coefficient of 22 $dm^3mol^{-1}\ cm^{-1}$ corresponding to a cross-section of $8.4 \times 10^{-20}\ cm^{-2}$. From the integrated absorption we deduce an oscillator strength $f = 2.0 \pm 0.1 \times 10^{-4}$ indicating that the electronic transition responsible for the blue colour of this gas is of the same type (n,π^*) as in CF_3NO and CH_3NO.[19,26,27] The structure clearly discernible on the long wavelength side of the spectrum is vibrational and mirrors transitions between torsional levels in the ground and elec-

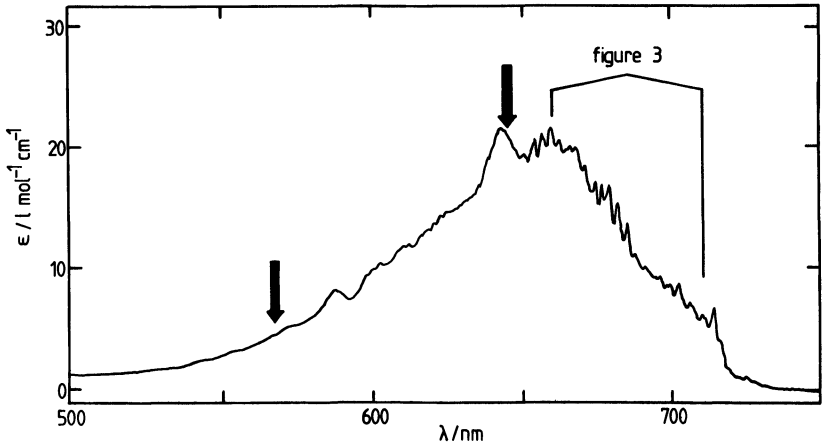

Figure 2 Electronic absorption spectrum of $CClF_2NO$ vapour at 295 K. The two wavelengths chosen for the room temperature photodissociation studies (645 and 568 nm) and the region of the LIF excitation spectrum of the jet-cooled molecule (Figure 3) are indicated by bold arrows and thin lines, respectively.

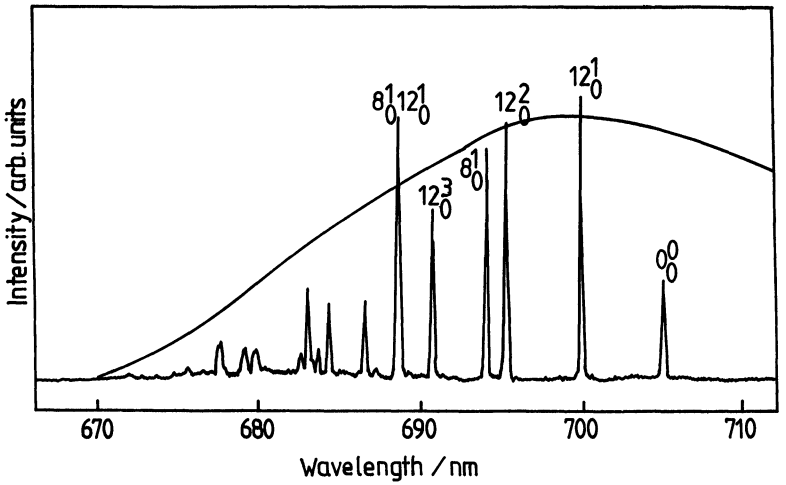

Figure 3 LIF fluorescence excitation spectrum of jet-cooled $CClF_2NO$.

tronically excited state. Due to the bent CNO grouping two distinct conformers with the O atom eclipsing either an F or a Cl atom are expected to be present at 300 K.[22] They execute large amplitude torsional vibrations within potential wells separated by barriers in the range 200–1000 cm^{-1}. The associated torsional levels are only spaced some 70 cm^{-1} apart and are highly unharmonic.[12,22,28] Near 300 K a large fraction of the thermal population occupies "hot" torsional levels. In conjunction with the eclipsed-staggered conformational change on electronic excitation that is characteristic for this class of molecules,[19,26–29] progressions in the torsional mode are observed, that lead to marked vibrational congestion at 300 K. This "hot" band congestion is more pronounced than the sequence congestion commonly encountered in aromatic systems since the Franck-Condon factors for out-of-phase or minimum to maximum electronic transitions v', v'' increase rapidly with increasing torsional quantum number v''.[27] On cooling to 200 K the spectrum sharpens up considerably indicating clearly that the apparent broadening or diffuseness is due to thermal congestion.

Figure 3 shows the LIF excitation spectrum of $CClF_2NO$ jet-cooled with Ar. Since the parent molecule emits fluorescence with lifetimes up to a few hundred ns, the predissociation of this molecule near the electronic origin indicated in Figure 3 is three orders of magnitude

slower than the predissociation of O, N and S-nitroso compounds in the near-UV.[8–11] The fluorescence excitation spectrum of jet-cooled $CClF_2NO$ has been recorded and discussed previously by Ernsting.[28] We have re-examined it and have studied the fluorescence decay of a range of single vibronic levels as part of a systematic investigation of the spectroscopy and photophysics of these compounds.[29] While we agree with the previous assignment of the electronic origin and of the major features of the spectrum, we have deduced substantially different potential curves for the ground and excited state. The conformational analysis of the $\tilde{A}$ and $\tilde{X}$ states of $CClF_2NO$ is beyond the scope of the present work and will be reported in detail elsewhere.[29] Briefly, we conclude, that the excitation spectrum of the jet-cooled molecule is carried almost entirely by a single energetically favoured but two-fold degenerate "gauche" conformer with the O atom eclipsing either of two equivalent F atoms in the $\tilde{X}$ ground state. The 300 K spectrum is also dominated by the gauche ground state rotamer but the *cis*-rotamer contributes roughly 15% of the integrated absorption. We have found

Table I Uncorrected wavelengths, transition wavenumbers $\tilde{\nu}$, intervals and assignments of the n,π^* LIF excitation spectrum of jet-cooled $CClF_2NO$ in the visible

λ/nm	$\tilde{\nu}$/cm^{-1}	$\Delta\tilde{\nu} = \tilde{\nu} - \tilde{\nu}_{00}$/cm^{-1}	Assignment
708.2	14119.7	−70.7	12_1^0
704.7	14190.4	0.0	0_0^0
699.5	14295.9	105.5	12_0^1
695.5	14378.1	187.7	—
694.8	14392.2	201.8	12_0^2
693.6	14417.5	227.1	8_0^1
691.0	14471.8	281.4	—
690.3	14486.5	296.1	12_0^3
688.2	14530.7	340.3	$8_0^1 12_0^1$
686.8	14560.3	369.9	—
686.1	14575.1	384.7	12_0^4
683.9	14622.0	431.6	$8_0^1 12_0^2$
683.2	14637.0	446.6	—
682.9	14643.4	453.0	—
682.6	14649.9	459.5	$7_0^1 12_0^1$
682.2	14658.5	468.1	—
679.4	14718.9	528.5	$8_0^1 12_0^3$
678.8	14731.9	541.5	—
677.2	14766.7	576.3	—
676.8	14775.4	585.0	—
675.3	14808.2	617.8	—
674.5	14825.8	635.4	—

no evidence for dimerisation or polymerisation of the parent in the jet under our expansion conditions as mentioned previously.[12]

Emission can only be excited in the small portion of the absorption spectrum close to the electronic origin of the transition as indicated in Figure 2, and rapid non-radiative processes clearly dominate the photophysics of the molecule at wavelengths shorter than 650 nm.

Table I summarises the assignment of the major features in the fluorescence excitation spectrum of $CClF_2NO$. The detailed vibrational analysis will be given elsewhere.[29] Normal mode 12 is the lowest a'' (in C_s symmetry) vibration and corresponds to the torsion. Modes 8 and 7 are the lowest frequency in-plane (a' in C_s symmetry) skeletal bending/rocking modes.

Photodissociation at 300 K

The two wavelengths 645 and 568 nm chosen for the photodissociation experiments with the 300 K vapour are indicated in the absorption spectrum of Figure 2 by bold arrows. The spectral congestion clearly precludes any state selection. At both wavelengths nascent $NO(X^2\Pi_i)$ was identified readily by the characteristic γ(O,O) two-photon LIF band near 450 nm. By changing the delay between pump (dissociation) and probe pulses we established that the formation of NO at both dissociation wavelengths occurs within the dissociation pulse (5 ns). An initial sharp rise due to the appearance of the fragment is followed by a slow decrease associated with diffusion out of the observation region and reaction. At these wavelengths the rates of appearance of NO can therefore not be measured with our equipment. By scanning the probe-laser through the $A^2\Sigma^+(v' = 0) \leftarrow X^2\Pi_i(v'' = 0)$ two-photon transition of NO with a fixed delay of 50 ns we recorded rotationally resolved two-photon excitation spectra of the nascent fragment. Collisional relaxation effects were shown to be negligible by examining the effect of increasing temporal delay between pump and probe pulses on the relative intensity of the well isolated O_{12}-branch near 454.5 nm. We were unable to detect $NO(v'' = 1)$ in the 645 nm photolysis.

Relative spectral intensities in the two-photon LIF excitation spectra were converted to rotationally resolved population distributions by means of the relationship

$$I_{rel} = C\, q_{v'v''}\, S_{J'J''}\, \bar{\nu}\, n_J/g_J$$

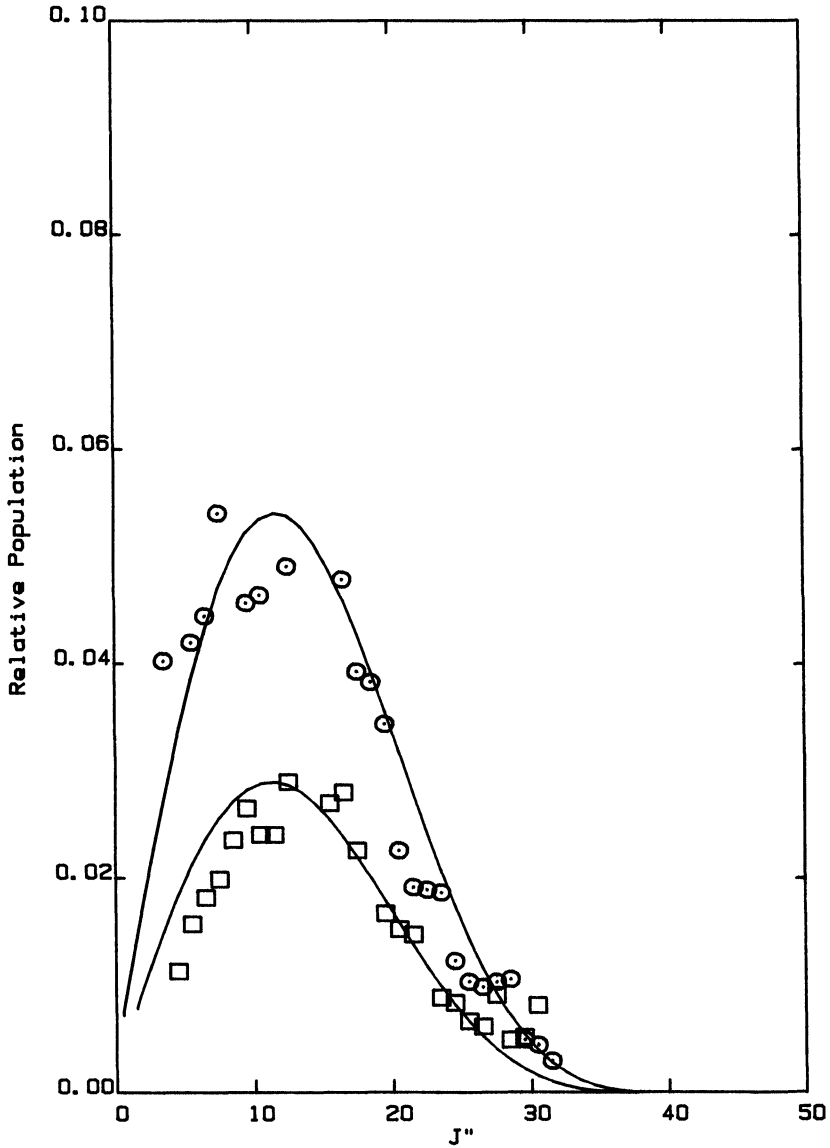

Figure 4 Rotational distributions of NO($v'' = 0$) from the photolysis of 300 K $CClF_2NO$ at 645 nm. The solid lines show calculated statistical distributions except for the spin-orbit ratio, which has been scaled to permit better comparison with experiment.

○, $X^2\Pi_{1/2}$ (F_1); □, $X^2\Pi_{3/2}$ (F_2)

where C is a constant, $q_{v'v''}$ stands for the Franck–Condon factor of the particular γ-band of NO, $S_{J'J''}$ for the two-photon Hönl–London factor and $\bar{\nu}$ for the wavenumber of the transition. $g_J = 2J + 1$ denotes the rotational degeneracy of the ground-state levels. Details of this method and of the two-photon LIF spectrum of NO have been given previously.[6,7,25] Since the predissociation studied here is slow on the timescale of the parent rotation, the photofragments cannot be aligned, and the spatial distribution of NO is isotropic. Observed line intensities were corrected for variations in the dissociation and probe laser power as well as for variations in the pressure of the parent molecules during the extensive spectral scans, that were necessary to record complete bands.

Figure 4 shows the NO($v'' = 0$) population distribution obtained in this way from the photolysis of $CClF_2NO$ at 645 nm and 300 K. While NO($v'' = 1$) is absent at 645 nm, a significant fraction of NO(X) formed in the 568 nm photolysis appears as NO($v'' = 1$). In both cases, the product-state distributions are dominated by low-J populations, and the spin-orbit population distributions are cold and not equilibrated.

Photolysis at 645 nm is well behaved and shows a linear dependence of the NO signal on dissociation pulse energy. Log-log plots of NO signal measured at the band head of the $P_{11} + O_{21}$ two-photon branch versus pulse energy are linear and provide a slope of 1.0 ± 0.1 at 645 nm and slope of 2.0 ± 0.1 at 568 nm as shown in Figure 5. Clearly, two or possibly more photons must be involved in the absorption step prior to dissociation at 568 nm.

To simulate statistical product-state (Prior) distributions we used a procedure outlined in a previous publication[19] and adapted from Bogan and Setser.[30] The probability for formation of NO in a given quantum state is calculated using energy conservation but neglecting angular momentum conservation, and by evaluating the density of product states for different available excess energies E^+. The vibrational frequencies of the $CClF_2$ radical are available from the matrix isolation studies of Milligan *et al.*[31] and Prochaska and Andrews.[32] The average parent internal energy was estimated using the known vibrational frequencies[22] and classical statistical mechanics.

Calculations were performed with the excess available energy E^+ as the only variable until the average rotational energy coincided with the experimentally observed value. Errors introduced by neglecting the strict angular momentum conservation of more sophisticated

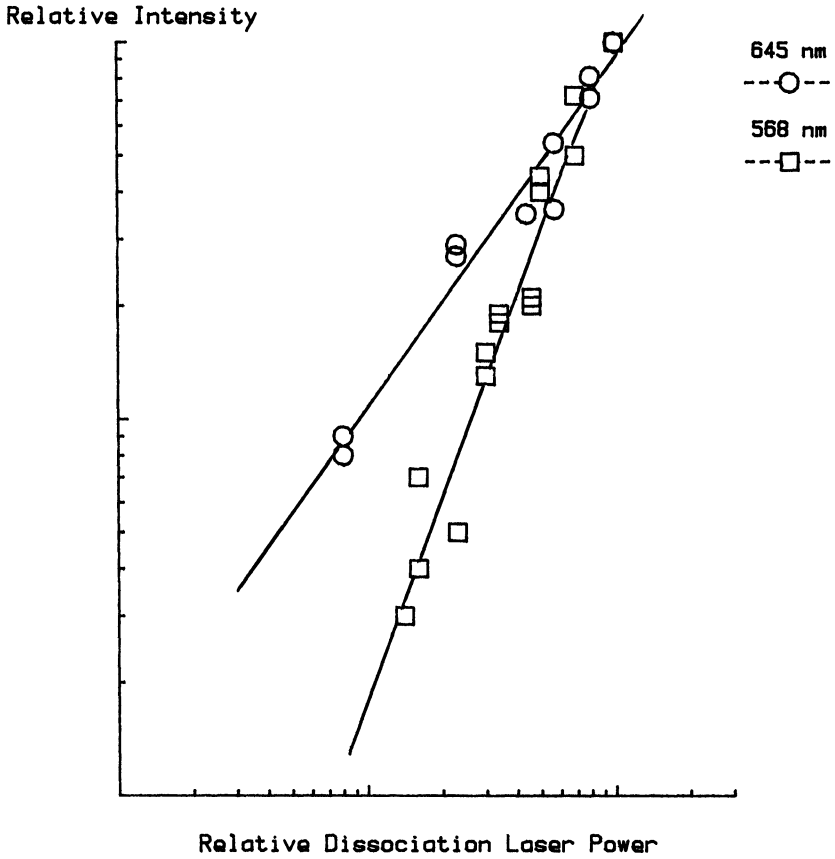

Figure 5 Log-log plot of the NO two-photon LIF signal excited on the band head of the $P_{11} + O_{21}$ branch near 452.3 nm *versus* 645 nm photolysis pulse energy.

approaches like phase space (PST) or statistical adiabatic channel theory (SACT) are likely to be minor in comparison to the errors associated with the uncertainty of the vibrational properties and the structure of the $CClF_2$ radical.

Experimental and calculated average rotational energies were evaluated by summation

$$\langle E_{\text{rot}} \rangle = \sum_{J,\Omega} n_J E_{\text{rot}} / \sum_{J,\Omega} r_J$$

Table II Photodissocation of 300K $CClF_2NO$: Observed and (in brackets) calculated average rotational ($\langle E_{rot} \rangle$) and vibrational ($\langle E_{vib} \rangle$) energies and spin-orbit ratios of the nascent NO photoproduct formed by pulsed photolysis at the wavelengths λ_{diss} · E^+ are the excess energies above the dissociation threshold used in the statistical calculations (see text).

λ_{diss} = 645 nm		λ_{diss} = 568 nm
$\langle E_{rot} \rangle / cm^{-1}$	391 (392)	580 (585)
$\langle E_{vib} \rangle / cm^{-1}$	<19 (4)	24 (57)
$F_1/F_2(v'' = 0)$	2.01 (1.35)	1.30 (1.24)
E^+	2600	4300

using the constants and term values for the intermediate coupling case to evaluate the rotational level energies E_{rot}. The spin-orbit ratios given are similarly obtained by summation

$$F_1/F_2 = \sum_{\Omega=1/2} n_J / \sum_{\Omega=3/2} n_J$$

Table II summarises observed and calculated E, V and R energy disposal into nascent NO in the photodissociation of $CClF_2NO$ at the two wavelengths.

Photodissociation in the free jet

The use of two separate electronically synchronised dissociation and probe laser systems permits one to carry out three distinct types of measurement with predissociating jet-cooled nitroso compounds. By scanning the dissociation laser through the structured absorption features of the cold parent while monitoring the undispersed fluorescence of the NO photoproduct excited at a fixed resonant wavelength of the probe laser, a photofragment yield spectrum can be obtained. Appearance rates of NO can be measured by varying the delay between dissociation and probe pulses, and finally, excitation spectra of the NO(X) photoproduct and hence product-state distributions can be recorded by scanning the probe laser, while keeping the dissociation wavelength fixed on the parent transition selected using a fixed electronic delay.

Figure 6 presents the photofragment yield spectrum of jet-cooled $CClF_2NO$ obtained by monitoring NO near 452.3 nm on the $P_{11} + O_{21}$ band head of the γ(O,O) two-photon transition. The spectrum was

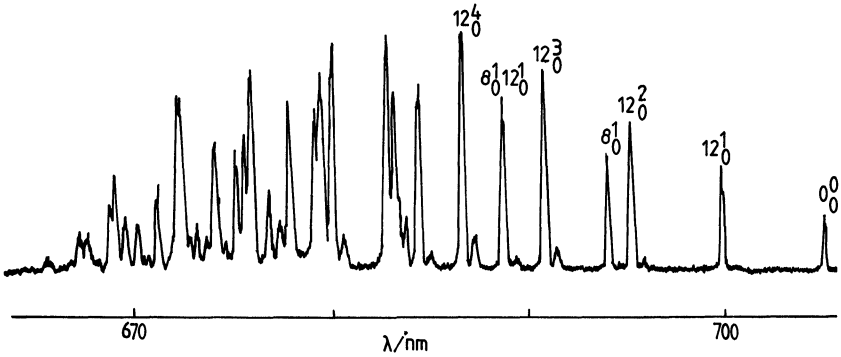

Figure 6 NO($X,v'' = 0$) photofragment yield spectrum of jet-cooled $CClF_2NO$. The probe laser excites the $P_{11} + O_{21}$ band head of the γ(O,O) $A^2\Sigma^+ \leftarrow {}^2\Pi_i$ two-photon transition near 452.3 nm while the dissociation laser is tuned through the absorption bands of the jet-cooled parent.

obtained with a delay of 100 ns between the dissociation and probe pulses, and consequently features at wavelengths longer than 680 nm may be progressively attenuated and may appear weaker as the NO appearance times become longer with decreasing excitation energy. Any parent lost by flying out of the focal region of the probe beam before dissociation will not contribute to the NO signal. A detailed comparison of the LIF excitation spectrum (Figure 3) and the photofragment yield spectrum leads us to conclude that there are no drastic differences that might indicate state specific effects.

In spite of the complications associated with fly-out effects and the use of a focused probe beam, we selected a number of vibronic features for estimating crude NO appearance rates from plots of the NO yield versus the delay time. The results of these measurements are collected in Table III. They are only meant to indicate general trends, and no firm conclusions can be drawn from this data. Under the free-jet conditions used parent molecules will cross the 0.1 mm focal region of the probe laser beam in roughly 100 ns. Thus, molecules dissociating on a time scale longer than this, move out of the observation region, and NO subsequently produced does not contribute to the signal. Houston and, subsequently, Reisler, Wittig and their respective collaborators were able to overcome this experimental problem by using single-photon LIF and wide unfocused probe beams[18,20] enabling them to measure NO appearance times well in excess of 200 ns. In our case

Table III Kinetics of the appearance of nascent NO following the state-selected photodissociation of jet-cooled $CClF_2NO$ at the wavelengths λ_{dis}/nm (transition wavenumber $\tilde{\nu}$). τ_{rise} -rise time of the NO appearance curve

λ_{diss}/nm*	Assignment	$\tilde{\nu}$/cm^{-1}	τ_{rise}/ns
704.7	0_0^0	14190	⩾240
699.5	12_0^1	14296	⩾230
694.8	12_0^2	14393	160
690.35	12_0^3	14485	⩾200
686.1	12_0^4	14575	180
682.6	$7_0^1 12_0^1$	14650	170
679.4	$8_0^1 12_0^3$	14719	140
677.2	—	14767	80
675.2	—	14810	90
671.6	—	14890	40
668.3	—	14963	40
664.9	—	15040	30
663.5	—	15072	40
661.1	—	15126	40
656.65	—	15229	20
651.3	—	15354	15
646.6	—	15466	<10
641.8	—	15580	<10

* Uncorrected.

the values collected in Table III give a reasonable estimate of the fast NO appearance rates ($\tau_{rise} < 100$ ns) but any slow component of a bi-exponential rise curve would be missed under our conditions. Risetimes longer than 100 ns quoted in Table III should be considered as lower limits only. Nevertheless, we may conclude, that the rate of appearance of NO increases monotonically with excitation energy, and for most vibronic transitions studied, the mean appearance times exceed the duration of the dissociation pulses.

Having obtained rough NO appearance times, energy disposal into rotation, the product-state distributions and electronic branching ratios of nascent NO($v'' = 0$) were measured. Figure 7 presents a section of a typical two-photon LIF spectrum of nascent NO($v'' = 0$) from the photolysis of $CClF_2NO$ on the strong feature at 646.6 nm. Low J transitions clearly dominate the spectra. In the example shown in Figure 7, band heads associated with the O_{11} and $P_{11} + O_{21}$ branches dominate the spectrum, whereas the O_{12} and $O_{22} + P_{12}$ band heads at longer wavelengths are much weaker. This indicates qualitatively, that NO is formed preferentially in the F_1 ($^2\Pi_{1/2}$) state. We recorded complete γ(O,O) two-photon LIF spectra of nascent NO($v'' = 0$) from

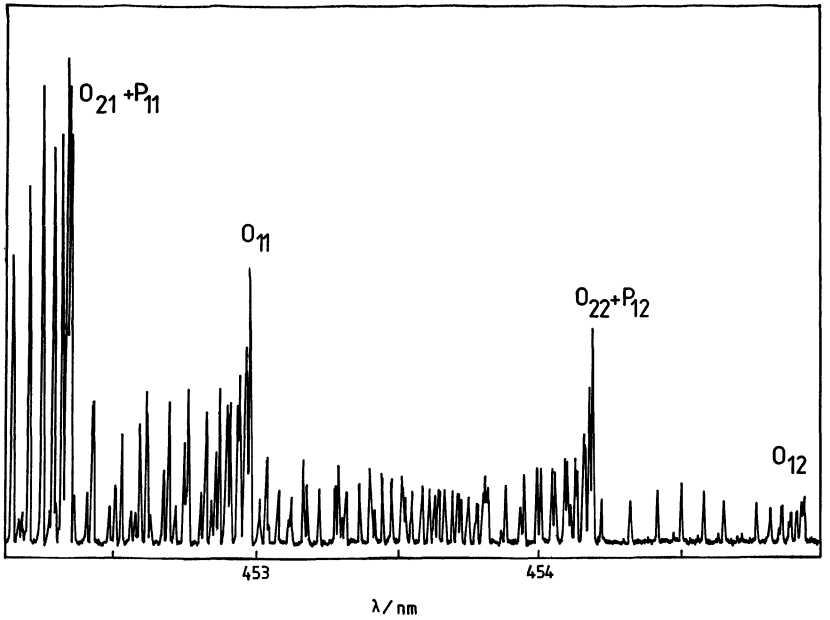

Figure 7 Section of the $A^2\Sigma^+$ ($v' = 0$) $\leftarrow$ $X^2\Pi_i$ ($v'' = 0$) two-photon LIF excitation spectrum of nascent NO from the photolysis of the jet-cooled parent molecule on the unassigned 646.6 nm vibronic transition.

the photodissociation of $CClF_2NO$ from 14 single vibronic levels of the $\tilde{A}(n,\pi^*)$ state and evaluated average rotational energies $\langle E_{rot} \rangle$ and spin-orbit ratios F_1/F_2 from the population distributions deduced as described above. Table IV summarises the results of this considerable experimental effort and also includes calculated statistical F_1/F_2 ratios and the excess energies E^+ required to fit statistical (Prior) distributions to the observed rotational product-state distributions. Comparisons of typical observed and simulated distributions are shown in Figures 8 and 9. Note, that the observed F_1/F_2 distributions are cold showing a clear non-statistical preference for the lower F_1 ($^2\Pi_{1/2}$) component. The calculated statistical distributions in Figures 8 and 9 have been scaled to the experimental n_J versus J distributions to permit better comparison. The Prior F_1/F_2 ratios are much closer to unity as evident from Table IV. These results clearly show that more energy appears in NO rotation as excess energy increases, but that the spin-orbit ratio remains non-statistical and very cold showing no sign

Table IV Photodissociation of jet-cooled $CClF_2NO$ following the state-selective excitation on wavelengths $\lambda_{diss} \cdot E_{exc} = \tilde{\nu} - \tilde{\nu}_{00}$ – energy above the lowest vibrational level of the $\tilde{A}(n,\pi^*)$ state. $\langle E_{rot} \rangle$ – average rotational energy of nascent NO($v'' = 0$). F_1/F_2 – experimental and calculated statistical spin-orbit ratios of nascent NO($v'' = 0$), E^+ – excess energy required to reproduce within ± 50 cm^{-1} the observed average rotational energies of NO with a statistical (Prior) model.

λ_{diss}/nm[a]	E_{exc}/cm^{-1}	$\langle E_{rot} \rangle$/cm^{-1} [b]	F_1/F_2 exp.	F_1/F_2 calc.	E^+/cm^{-1}
699.5	106	219	2.79	1.61	1300
694.8	202	227	3.12	1.61	1300
690.35	296	260	4.23	1.51	1600
682.6	460	249	4.19	1.57	1400
675.18	620	371	2.79	1.37	2400
671.6	699	323	3.59	1.41	2100
668.3	773	279	2.57	1.49	1700
664.9	849	344	4.10	1.40	2200
663.5	881	294	3.39	1.46	1800
661.1	936	352	3.66	1.34	2700
656.65	1038	340	3.43	1.40	2200
651.3	1164	339	4.06	1.40	2200
646.6	1275	393	3.03	1.35	2600
641.8	1391	325	3.16	1.38	2300

[a] Uncorrected wavelengths.
[b] Estimated uncertainty: ±10%.

of approaching 1. For all of these experiments the absorption/dissociation process was fully saturated *i.e.* the NO signal became independent of the dissociation pulse energy. At low dissociation power, however, a single-photon laser power dependence became apparent as shown in Figure 10. Since the product-state distributions were found to be independent of the dissociation pulse energy, we are confident that multiphoton absorption and dissociation (MPD) do not contribute to the results obtained with jet-cooled $CClF_2NO$.

C–N bond dissociation energy

Dissociation-probe experiments provide an interesting opportunity to determine C—N bond dissociation energies of jet-cooled, nearly monoenergetic C-nitroso compounds.[18–20] Two approaches are feasible for estimating D_0(C—N) from the observed energy disposal into NO as outlined previously.[19] The excess energy available at a given

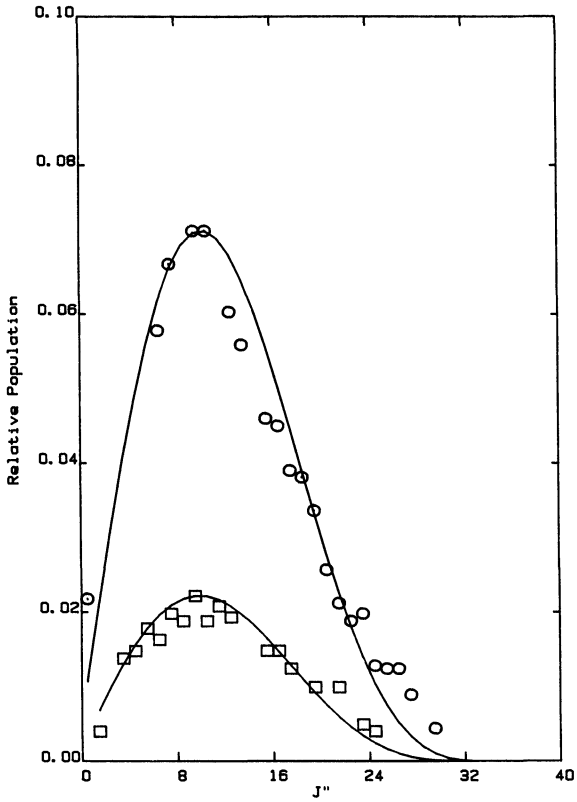

Figure 8 Observed and calculated statistical rotational distributions of the nascent NO($v'' = 0$) photoproduct from the dissociation of jet-cooled $CClF_2NO$ on the 663.5 nm vibronic feature. For additional explanations see legend of Figure 4.

photolysis wavelength E^+ may be identified by locating the highest rotational state of the nascent NO fragment. Due to the poor sensitivity of the two-photon LIF probe technique these thresholds were buried in noise and could not be located with confidence. The less accurate alternative approach demonstrated first by Bower *et al.*[18] in the case of CF_3NO had to be used. Here the excess energies E^+ available for a statistical disposal into the photofragments are estimated by fitting Prior distributions to rotational product-state distributions observed at several photolysis wavelengths. A D_0(CN) value of 13 700 ± 350 cm^{-1} or 164 kJ mol^{-1} was obtained from the intercept of E^+ *versus* the excitation energy.

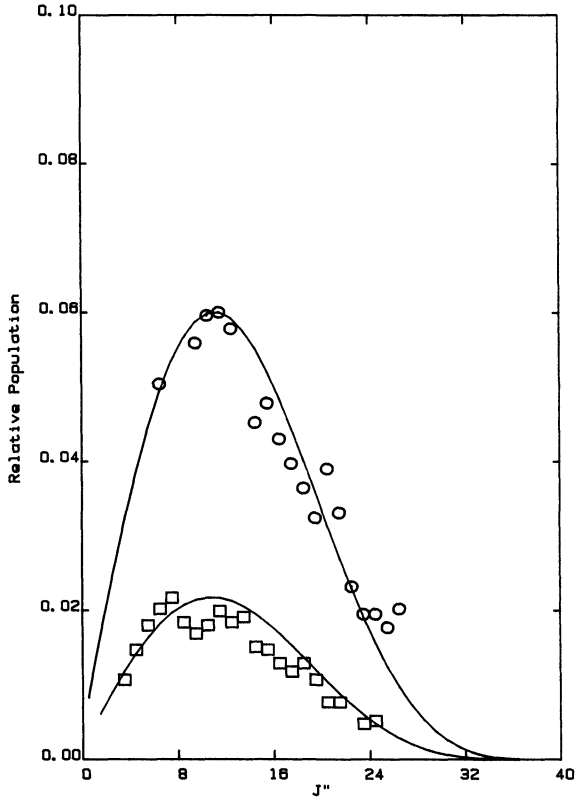

Figure 9 Observed and calculated statistical rotational distributions of nascent NO($v'' = 0$) from the photolysis of the jet-cooled parent at 641.8 nm. For additional explanations see legend of Figure 4.

DISCUSSION

Our results of the photolysis of $CClF_2NO$ at ambient temperature indicate a substantial dependence of the dissociation mechanism on the wavelength. At 645 nm the expected single-photon process dominates as judged from the dependence of the NO yield on pulse energy. The statistical model reproduces energy disposal into the rotation and vibration of NO reasonably as shown in Table II, and the rotational population distribution of NO agrees well with a statistical distribution calculated with an excess energy E^+ of 2600 cm^{-1}. The 568 nm

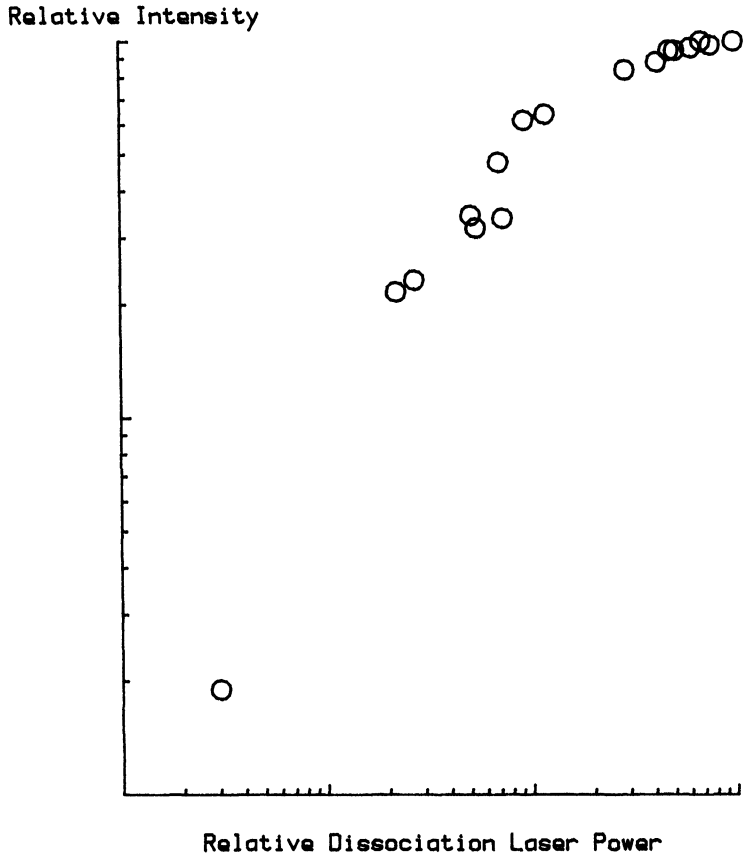

Figure 10 Log-log plot of the NO two-photon LIF signal excited near 452.3 nm *versus* dissociation pulse energy at 694.8 nm (12^2_0 vibronic transition).

photodissociation, in contrast, leads to a rotational population distribution, that can only be simulated poorly, and much less energy appears in the vibration of NO than predicted by the model. This may imply, that energy disposal at this wavelength may have some dynamical basis. The spin-orbit distributions are too cold at either wavelength to mirror a statistical disposal of excess energy into the electronic degree of freedom of the NO product. The higher order power dependence observed at 568 nm indicates that dissociation *via* S_1 and *via* a higher state reached by sequential absorption of another

photon leads to competition between quite unrelated dissociation channels.

The comparison of our results for the photodissociation of $CClF_2NO$ at 300 K and in the jet clearly shows the advantages of jet-cooling for achieving state-selective excitation and for studying the unimolecular decomposition of monoenergetic excited molecules. The data on energy disposal in the photodissociation of $CClF_2NO$ following excitation of well defined single vibronic levels of the $\tilde{A}(n,\pi^*)$ state (Table IV) show that the average energy appearing as rotation of NO increases with increasing available energy. There are no abrupt changes that might indicate state-specific effects, as the vibrational character of the initially excited level changes, and the observed product rotational distributions conform very well to statistical distributions as evident by the comparison between calculated and observed distributions in Figures 8 and 9. Even at the highest excess energy, ca 1900 cm^{-1} above the dissociation threshold, we cannot see any clear indication of non-statistical or dynamical effects in the NO rotational distribution. The spin-orbit distributions, however, are far too cold to reflect a statistical partitioning of excess energy and remain cold even at the highest excess energies involved. Similar product-state distributions for nascent NO are found in the case of CF_3NO, where only slight deviations from statistical n_J-distributions appear at high excess energy, and where the F_1/F_2 ($\Pi_{1/2}/\Pi_{3/2}$) ratios remain high.[18,19] In the photodissociation of $(CH_3)_3CNO$, on the other hand, Noble *et al.* were able to distinguish two excitation regions leading to distinctly different NO product-state distributions.[20] Here, dissociation near threshold apparently proceeds on S_0 on a time scale >3.5 μs and yields NO with a statistical product-state distribution, while fast predissociation via the triplet state T_1 predominates from S_1 levels located more than 650 cm^{-1} above threshold. This rapid predissociation by intersystem crossing (ISC) gives rise to NO with decidedly cold and non-statistical rotational and spin-orbit distributions.

Wittig and collaborators have summarised possible reasons for cold-spin-orbit populations of the nascent NO from the predissociation of 2-methyl-2-nitrosopropane.[20] In our case the statistical nature of the NO rotational distributions indicates that there is no significant barrier in the exit channel leading to the fragments. The colder than statistical spin-orbit ratios, on the other hand, may be the consequence of the absence of strong coupling between the $\Pi_{1/2}$ and $\Pi_{3/2}$ surfaces

correlating parent and separated fragments. Alternatively, the branching is controlled by the dynamics of the nonadiabatic transfer associated with the crossing of potential energy surfaces.

The near-threshold dissociation of C-nitroso alkanes offers an interesting opportunity to study the unimolecular decomposition of long-lived, weakly bound complexes. By combining state-selective excitation with detailed mapping of product-state distributions, dissociation rate and fluorescence decay measurements, it is possible to obtain a fairly complete picture of the predissociation dynamics. Unfortunately our knowledge of the potential energy surfaces connecting the three relevant bound states of bent R—N=O $\tilde{X} = S_0$, $\tilde{A}(n,\pi^*) = S_1$ and $\tilde{a}(n,\pi^*) = T_1$ with the fragments is inadequate and rests entirely on the analogy with HNO, where the surfaces and correlations are known relatively well.[33] There are essentially three mechanisms that need to be considered in principle in the predissociation of RNO $\tilde{A}(n,\pi^*)$ where R is an alkyl group:

1) predissociation by internal conversion (IC) and unimolecular decomposition on the ground state surface (S_0).

2) predissociation by $S_1 - T_1$ intersystem crossing (ISC) and decay on the T_1 surface.

3) vibrational predissociation on an $\tilde{A}(n,\pi^*) = S_1$ surface, that is quasi-bound or has only a shallow minimum of a few hundred cm^{-1} along the dissociation coordinate.

Mechanisms 1 and 2 have been invoked previously,[8,12,18–20] but the third possibility has not hitherto been considered.

Houston and collaborators concluded from the statistical behaviour of the NO product rotation and the monotonic increase of the NO appearance and fluorescence day rate of $\tilde{A}$ state CF_3NO with excitation energy, that mechanism 1 predominates, but did not exclude a contribution from mechanism 2 at higher energy.[18] We have recently reported evidence for significant involvement of ISC (mechanism 2) and the importance of T_1 in the predissociation of CF_3NO. S_1 levels higher than 700 cm^{-1} above threshold appear to decay mainly by ISC. In the large molecule $(CH_3)_3CNO$ Noble *et al.* identified both mechanism 1 and 2 with the latter providing the dominant route for $E^+ > 650$ cm^{-1}. The predissociation of HNO $\tilde{A}^1A''$ from levels within 700 cm^{-1} of the dissociation threshold by mechanisms 1 and 2 is understood in

considerable detail based on the work of Dixon *et al.*[16,17,33] Mechanism 3 remains unimportant in HNO since a sizeable barrier separates the $\tilde{A}$ state minimum from the dissociation asymptote. The assumption that a similar barrier is present in the $\tilde{A}(n,\pi^*)$ states of C-nitroso compounds is probably incorrect. There is evidence that the $\tilde{A}$ states of C-nitrosoalkanes exhibit only very shallow potential minima along the minimum energy path leading to the separate fragments.[34] We conclude therefore, that mechanism 3 also needs to be considered for the near-threshold dissociation of $CClF_2NO$.

We have observed pronounced biexponential fluorescence decay behaviour for all $\tilde{A}(n,\pi^*)$ levels of $CClF_2NO$ situated higher than 200 cm^{-1} above the $v' = 0$ vibrational level[29] indicating strong mixing of these levels with T_1. ISC is therefore an important and for the higher levels probably the dominating pathway for the $\tilde{A}$ state predissociation, which must show the same temporal characteristics as the fluorescence decay. We anticipate therefore that the NO appearance curves will reveal a fast and slow component on careful measurement with a better technique than was available to us. In CF_3NO $\tilde{A}$ state levels higher than 700 cm^{-1} predissociate predominantly by ISC. In $CClF_2NO$ dissociation by mechanism 2, i.e. via ISC under the influence of spin-orbit coupling and in the absence of a significant barrier produces statistical rotational NO distributions. Levels close to the O,O electronic origin may decay either by IC (mechanism 1) or by vibrational predissociation (mechanism 3) on an S_1 surface with a very shallow minimum. The observed product-state distributions do not permit us to discriminate between these mechanisms.

CONCLUSION

The predissociation dynamics of $CClF_2NO$ $\tilde{A}(n,\pi^*)$ strongly resembles that of the parent molecule CF_3NO, and the dynamics of all but the lowest $\tilde{A}$ state levels is dominated by ISC. Levels close to the O,O origin of the $\tilde{A}$–$\tilde{X}$ system predissociate either by internal conversion or by direct vibrational predissociation on the weakly bound S_1 surface. Fluorescence decay measurements provide more information about the involvement of T_1 than the rotational and spin-orbit populations of the nascent NO photoproduct. Little evidence for state-specific behaviour is revealed by the monotonic dependence of the rotational

product-state distribution and energy disposal into rotation on the quantum state excited in the $\tilde{A}(n,\pi^*)$ state of the parent.

C-nitrosoalkanes offer the possibility of studying in detail the dissociation dynamics of weakly bound complexes. Fluorescence excitation and laser photofragment yield spectra provide information on the level structure and some information on the potential surface of the parent, while detailed dynamical information can be gleaned from time-resolved fluorescence and appearance rate measurement and NO product-state distributions.

Acknowledgements

We are grateful to the S.E.R.C. and its Laser Support Facility for a grant and the loan of laser equipment. We also thank the Carnegie Trust for the Universities of Scotland for a scholarship (to M.R.S.McC.) and the S.E.R.C. for an earmarked studentship (to J.A.D.) J.P. thanks the Royal Society of Edinburgh for a support fellowship.

References

1. J. P. Simons, *J. Phys. Chem.* **88,** 1287 (1984).
2. M. N. R. Ashfold and J. E. Baggott (eds.), "Molecular Photodissociation Dynamics," Royal Society of Chemistry, London, 1987.
3. G. E. Busch, J. R. Cornelius, R. T. Mahoney, R. I. Morse, D. W. Schlosser and K. R. Wilson, *Rev. Sci. Instrum.* **41,** 1066 (1970).
4. S. R. Leone, *Adv. Chem. Phys.* **50,** 255 (1982).
5. H. Zacharias, M. Geilhaupt, K. Meier and K. H. Welge, *J. Chem. Phys.* **74,** 218 (1981).
6. R. G. Bray, R. M. Hochstrasser and J. E. Wessel, *Chem. Phys. Lett.* **27,** 167 (1974).
7. J. B. Halpern, H. Zacharias and R. Wallenstein, *J. Mol. Spectr.* **79,** 1 (1980).
8. H. Reisler, M. Noble and C. Wittig, in ref. 2, p. 139.
9. M. R. S. McCoustra and J. Pfab, *Chem. Phys. Lett.* **137,** 355 (1987).
10. O. Benoist d'Azy, F. Lahmani, C. Lardeux and D. Solgadi, *Chem. Phys.* **94,** 247 (1985).
11. A. E. Bruno, U. Brühlmann and J. R. Huber, *Chem. Phys.* **120,** 155 (1988).
12. M. R. S. McCoustra, J. A. Dyet and J. Pfab, *Chem. Phys. Lett.* **136,** 231 (1987).
13. J. Pfab, J. Häger and W. Krieger, *J. Chem. Phys.* **78,** 266 (1983).
14. C. X. W. Qian, M. Noble, I. Nadler, H. Reisler and C. Wittig, *J. Chem. Phys.* **83,** 5573 (1985).
15. H. Reisler and C. Wittig, *Ann. Rev. Phys. Chem.* **37,** 307 (1986).
16. R. N. Dixon, K. B. Jones, M. Noble and S. Carter, *Mol. Phys.* **42,** 455 (1981).
17. R. N. Dixon, M. Noble, C. A. Taylor and M. Delhouse, *Faraday Discuss. Chem. Soc.* **71,** 125 (1981).
18. R. D. Bower, R. W. Jones and P. L. Houston, *J. Chem. Phys.* **79,** 279 (1983).
19. J. A. Dyet, M. R. S. McCoustra and P. Pfab, *J. Chem. Soc.* Faraday II, **84,** 463 (1988).
20. M. Noble, C. X. W. Qian, H. Reisler and C. Wittig, *J. Chem. Phys.* **85,** 5763 (1986).
21. A. V. Fokin, A. T. Uzun and Y. M. Kosyrev, *Zhurn. Obshch. Khim.* **36,** 540 (1966).

22. N. P. Ernsting and J. Pfab, *Spectrochim. Acta* **36A,** 75 (1980).
23. J. A. Dyet, PhD Thesis, Heriot-Watt University, Edinburgh, 1987.
24. M. R. S. McCoustra, PhD Thesis, Heriot-Watt University, Edinburgh, 1986.
25. M. R. S. McCoustra and J. Pfab, *J. Chem. Soc. Faraday 2,* **84,** 655 (1988).
26. N. P. Ernsting, J. Pfab and J. Römelt, *J. Chem. Soc., Faraday 2* **74,** 2286 (1978).
27. J. A. Dyet, M. R. S. McCoustra and J. Pfab, *Chem. Phys. Lett.* **135,** 534 (1987); and **137,** 398 (1987).
28. N. P. Ernsting, *J. Chem. Phys.* **80,** 3042 (1984).
29. J. A. Dyet, M. R. S. McCoustra and J. Pfab to be published.
30. D. J. Bogan and D. W. Setser, *J. Chem. Phys.* **64,** 586 (1976).
31. D. E. Milligan, M. E. Jacox, J. H. McAuley and C. E. Smith, *J. Mol. Spectr.* **45,** 377 (1973).
32. F. T. Prochaska and L. Andrews, *J. Amer. Chem. Soc.* **100,** 2102 (1978); and *J. Chem. Phys.* **68,** 5577 (1978).
33. S. Carter and R. N. Dixon, *Mol. Phys.* **55,** 701 (1985).
34. J. Pfab, *Faraday Discuss. Chem. Soc.* **82,** 204 (1986).